LASER INTERFEROMETER GRAVITATIONAL WAVE OBSERVATORY
– LIGO –

LIGO Laboratory / LIGO Scientific Collaboration

LIGO-T010075-00-D *ADVANCED LIGO* 27 June 2001

Advanced LIGO Systems Design

LIGO Scientific Collaboration, ed. P Fritschel

Distribution of this draft:

LIGO Scientific Collaboration

This is an internal working note
of the LIGO Project.

California Institute of Technology
LIGO Project - MS 51-33
Pasadena CA 91125
Phone (818) 395-2129
Fax (818) 304-9834
E-mail: info@ligo.caltech.edu

Massachusetts Institute of Technology
LIGO Project - NW17-161
Cambridge, MA 01239
Phone (617) 253-4824
Fax (617) 253-7014
E-mail: info@ligo.mit.edu

LIGO Hanford Observatory
P.O. Box 1970
Mail Stop S9-02
Richland, WA 99352
Phone 509-372-8106
Fax 509 372 8137

LIGO Livingston Observatory
P.O. Box 940
Livingston, LA 70754
Phone 225-686-3100
Fax 225-686-7189

http://www.ligo.caltech.edu/

1 INTRODUCTION

This document describes the system requirements and design for the Advanced LIGO detectors. It is intended to guide the development of the subsystem designs.

2 UPGRADE APPROACH

The proposal for the second generation interferometers is to upgrade the LHO 4 km and the LLO interferometers with instruments having improved broadband performance. Specific design choices and interferometer parameters are evaluated principally against their impact on the sensitivity to neutron star binary inspirals (NBI). In this sense the design is optimized for neutron star binary inspirals, but this also tends to give good broadband performance. Design choices are also made with consideration given to technical breakpoints–all feasible attempts are made to improve strain sensitivity, though there may be no significant improvement detection sensitivity of known sources. This approach is motivated by lack of knowledge of what gravitational wave signals the initial interferometers will detect, if any; designing the second generation interferometers to have improved broadband performance is thus judged to be the most prudent route to ‘discovery’.

In this scenario, every initial LIGO subsystem is upgraded, either to directly reduce one of the fundamental noise sources or to control technical noise sources. While there may be a staged approach to the installation and commissioning of the advanced subsystems, the scientific performance goal is not reached until the complete new design is implemented.

It is further proposed to upgrade the LHO 2 km interferometer to have a tunable, but relatively narrowband response, and to increase its length to 4 km. It would be designed to be sensitive at higher frequencies than the broadband interferometers, with a tuning range of roughly 500 Hz-1 kHz. The specific design of the third interferometer is not further defined at this time, however, and thus is not part of this document.

3 SYSTEM LEVEL REQUIREMENTS

3.1. Strain sensitivity

Figure 1 shows the current estimate of the equivalent strain spectrum of an advanced LIGO interferometer made with 40 kg sapphire test masses. It should be stressed that this an estimate of what may be attainable, and is used to performance requirements for the interferometer subsystems. Given present uncertainties in some of the parameters affecting the fundamental noise sources (particularly internal thermal noise), it is premature to specify a required overall strain sensitivity spectrum.

The main parameters affecting the fundamental noise sources are:

- *Quantum noise:* 125 W input power; 830 kW arm cavity power; homodyne (DC) readout; photodetector quantum efficiency, 90%
- *Internal thermal noise:* beam size on test masses, 6.0 cm radius; test mass *Q*, 200 million (no degradation from polishing or coating included)
- *Suspension thermal noise:* round fiber (actually square), sized to minimize ~20 Hz ther-

mal noise

- *Residual gas:* beam tube pressure, 10^{-9} torr, H_2

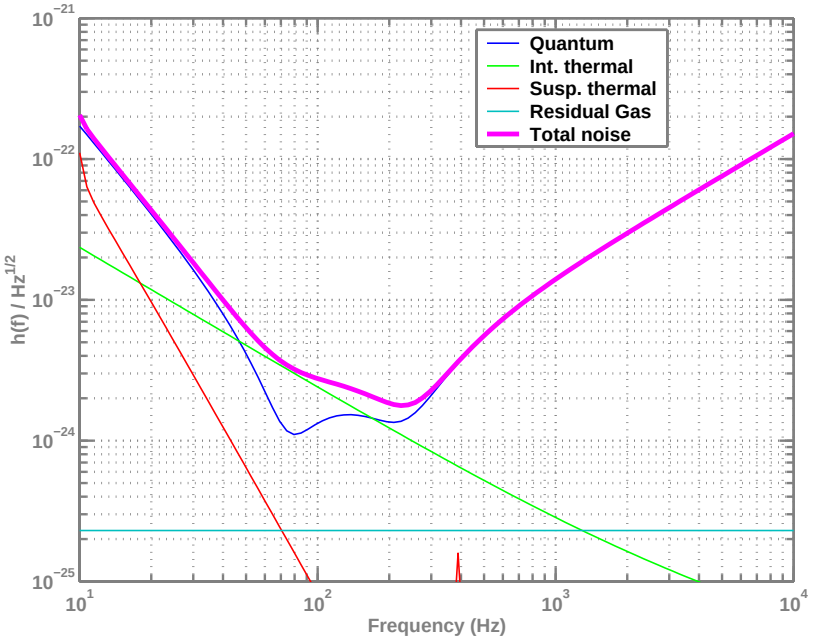

Figure 1. Current estimate of the advanced LIGO interferometer strain sensitivity, calculated using BENCH, v. 1.10. The design uses 40 kg sapphire test masses, signal recycling, and 125 W input power. The neutron-star binary inspiral detection range for a single such interferometer is 209 Mpc.

The strain sensitivity estimate for an interferometer using fused silica test masses is given in Appendix A.

3.2. Non-gaussian noise

Care must be taken in designing the interferometer subsystems to avoid potential generation of non-gaussian noise (avoiding highly stressed mechanical elements, e.g.).

3.3. Availability

The availability requirements for initial LIGO, specified in the *LIGO Science Requirements Document*, E950018-02-E, are applied to the advanced LIGO interferometers; in short:

- 90% availability for a single interferometer (integrated annually); minimum continuous operating period of 40 hours
- 85% availability for two interferometers in coincidence; minimum continuous operating period of 100 hours
- 75% availability for three interferometers in coincidence; minimum continuous operating period of 100 hours

3.4. Environmental sensing

The environment will be monitored with initial LIGO's Physical Environmental Monitoring (PEM) system. No additional monitoring functions are expected to be required, though it is possible that some of the sensors will be upgraded.

3.5. Infrastructure constraints

The advanced interferometers must be implemented within the existing LIGO facilities. There will be no significant changes to the buildings or vacuum system, with the following possible exceptions:

- the mode cleaner vacuum tube (connecting HAM1(7) with HAM2(8)) may be replaced with a larger diameter tube, if the additional clear aperture is found to be required to pass the various laser beams
- the mid-station BSC chambers at LHO may be moved to the end-stations, so that all three interferometers would have 4 km arm lengths

3.6. Data acquisition: channels & timing

The sampling rate and timing requirements for the data acquisition system are the same as for initial LIGO (sampling rate for the gravitational-wave channel is 16384/sec; other rates are channel-dependent). Each subsystem must be designed with appropriate data acquisition channels, such that the performance of the subsystem and its influence on the gravitational-wave signal can be diagnosed.

4 SYSTEM LEVEL DESIGN

This section describes the system level design choices that have been made or are under consideration. The basic interferometer design is shown in Figure 2. In addition to the fact that the initial LIGO interferometer subsystems are upgraded, several new elements have been added to the design; these are motivated and discussed first in this section. Then the choices for the major interferometer parameters are examined.

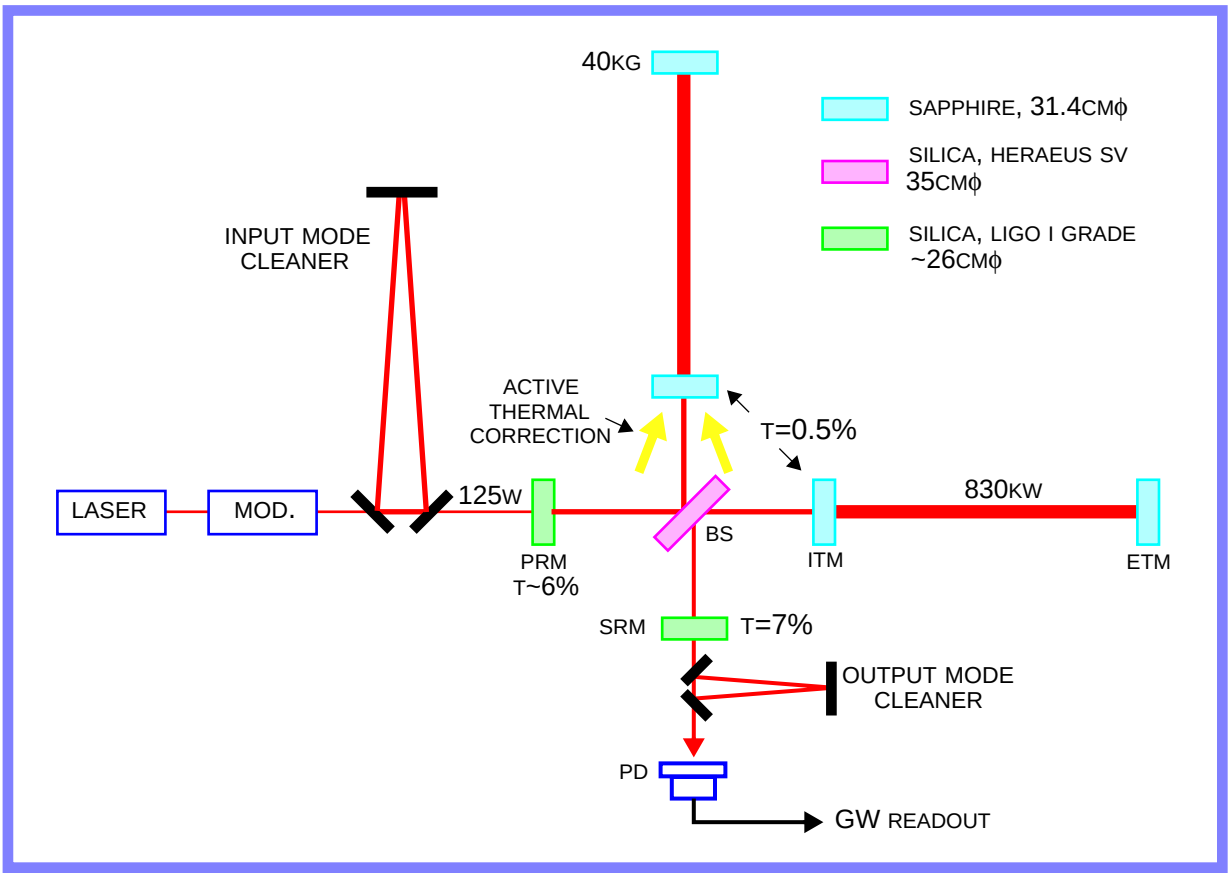

Figure 2. Basic layout of an advanced LIGO interferometer.

4.1. Signal recycling configuration

The configuration of the advanced interferometers is a power-recycled and signal-recycled Michelson interferometer with Fabry-Perot cavities in the arms–i.e., initial LIGO, plus signal recycling. Mirror reflectivities are chosen based on thermal distortion and other optical loss estimates, and according to the optimization of NBI detection. To limit system complexity, the signal recycling is not required to have broad tuning capability *in situ* (i.e., no compound signal recycling mirror; nor any kind of 'multi-disc cd player' approach, involving multiple signal recycling mirrors on a carousel), though it may have some useful tunability around the optimal point.

The principal benefit of signal recycling is the ability to reduce the optical power in the substrates of the beam splitter and arm input mirrors, thus reducing thermal distortions due to absorption in the material. To illustrate this advantage, the baseline design can be compared with a non-signal-recycled version, using the same input laser power but with mirror reflectivities re-optimized. The signal recycled design has a (single interferometer) NBI range of 200 Mpc, with a beamsplitter power of 2.1 kW; the non-SR design has a NBI range of 180 Mpc, but with a beamsplitter power of 36 kW. Alternatively, if the beamsplitter power is limited to 2.1 kW, the non-SR design would have a NBI range of about 140 Mpc.

The limit to increasing the arm cavity finesse and correspondingly lowering the Michelson power is loss in the signal recycling cavity, which limits the degree to which signal sidebands can be recycled back into the arms. The most significant of these losses may be due to mode mismatch between the arm cavity mode and the signal recycling cavity mode; other losses come from AR surfaces of the input mirrors and beamsplitter, and imperfect interference at the beamsplitter.

4.2. Output mode cleaner

The second new component in the design is an output mode cleaner. The principal motivation to include this is to limit the power at the output port to a manageable level, given the much higher power levels in the interferometer compared to initial LIGO. For the dc readout scheme (see ...) the output mode cleaner is necessary to limit the technical amplitude noise on the light.

The 20× higher input power does not scale directly to 20× higher output power though. Signal recycling allows us to lose a larger fraction of the power in the arms, so that the power at the beamsplitter is only 10× higher in advanced LIGO. Furthermore, the signal recycling mirror will suppress the higher-order modes on the antisymmetric side of the beamsplitter by a factor of ~5 or so. The output carrier power may thus be only 2-3× higher than initial LIGO, or ~0.2-0.4 W. Local oscillator power would bring the total output power to ~1-few watts.

With an output mode cleaner all but the TEM_{00} component of the contrast defect would be rejected by a factor of ~1000, leaving of order 1 mW of carrier power, ~10 mW including the local oscillator. This makes the dc readout scheme viable, and greatly eases the sensing and laser noise requirements for an rf heterodyne readout. With a dc readout, the mode cleaner would be a short (~1 m) triangular rigid cavity; an rf readout would require a longer cavity to pass the rf sidebands, composed of individually suspended mirrors. In either case the OMC will be mounted in-vacuum on a HAM isolation platform(s), and will have a finesse of order 100 to give high transmission (>99%) for the TEM_{00} mode and high rejection (>1000) of higher order modes.

4.3. Active thermal compensation

The final new component in the advanced LIGO design is a system for actively compensating thermal distortions arising from absorption in the core optics. Already for initial LIGO thermal lensing in the input test masses is a significant issue, and the recycling mirror curvature is deliberately altered (flattened) to prevent the hot recycling cavity from becoming unstable. The magnitude of the thermal problem in the advanced design depends on which test mass material is chosen, the extent to which absorption in the bulk material and the coatings can be improved. The

table below gives a comparison of the range of thermal loading. Only at the optimistic end of the

	Bulk absorption		*Surface*		*Total absorbed power, mW*	*Thermal constants (SiO_2/Al_2O_3)*	
	coeff., ppm/cm	*power, mW*	*coeff., ppm*	*power, mW*		κ	κ/α
Initial LIGO	5	12	0.6	10	22		
AdL, silica	0.5-1	10-20	0.1-0.5	50-320	60-340		
AdL, sapphire	10-40	260-1100	0.1-0.5	80-500	350-1600	0.04	0.45

Table 1. Comparison of thermal loading in the interferometers, with the thermal constants of sapphire, relative to fused silica. Thermal lensing is proportional to $1/\kappa$ and thermo-elastic distortion is proportional to α/κ. At the low end of the sapphire range, the optical path distortion is about 1.5× the initial LIGO level.

sapphire range might it be possible to operate without any active compensation. However we also require the interferometer to operate with 6× lower input power (see section 4.4.), which probably prevents us from figuring the recycling mirror for the hot conditions. We thus include active compensation in the baseline design, and will continue to evaluate its necessity.

Two methods of compensation are being pursued: a ring radiative heater located near the optic being compensated; an ex-vacuo heating laser beam, scanned over the optic. Both methods will be actively developed. The choice between (or a combination of) the two will be made as the material properties of the chosen test mass material become established; systems design issues will come into play regarding the level of compensation required.

Another systems issue regarding thermal compensation is the option of a compensation plate(s): a plate added between the beamsplitter and the input test mass, possibly one in each arm, on which the active compensation would be applied. Advantages of such compensation plates are:

- limits the temperature rise in the test mass: temperature rise with ring compensation, at the edge of the optic, is 30˚C/W absorbed for sapphire, 48˚C/W for silica
- greater flexibility interfacing the thermal actuator
- avoidance of any noise problems with a laser beam actuator

The disadvantages of course are those applicable to any additional in-vacuum components–space, design effort, cost. At this time, more study is needed of the benefits and potential designs of compensation plates to determine whether or not to include them in the baseline design.

4.4. Input power

The interferometer input power of 125 W is chosen based on considerations of power absorption and the point of diminishing returns for the NBI sensitivity. Figure 3 shows the NBI range versus input power for the reference design with sapphire test masses.

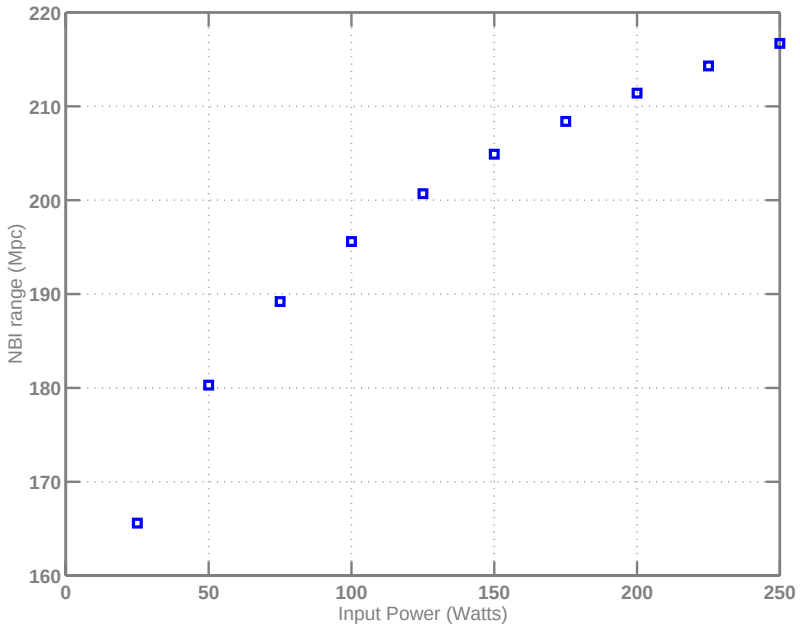

Figure 3. Neutron star binary inspiral range versus input power for the sapphire test mass reference design. The signal recycling mirror parameters are roughly optimized at each point. The design input power is 125 W.

At 125 W input power, the strain sensitivity from 10-40 Hz is dominated by the radiation pressure region of quantum noise. Thus better low frequency performance could be achieved by lowering the input power. To take advantage of this possibility[1], we require that the interferometer be designed to operate also at an input power of 20 W. At this level the quantum radiation pressure is at roughly the same level as the suspension thermal noise from 10-30 Hz, so yet lower power does not gain much. The stochastic background sensitivity (for a spectrum with constant energy density per logarithmic frequency interval) is improved by a factor of 3 at the lower input power (or a fac-

1. One might want to operate in such a mode with better low frequency performance but poorer sensitivity in the most sensitive region for increased sensitivity to a stochastic background of gravitational waves, or to black hole-black hole mergers of a certain intermediate mass range.

tor of 9 shorter integration time to achieve a given sensitivity level). The strain sensitivity for the sapphire reference design at 125 W and 20 W is shown in Figure 4.

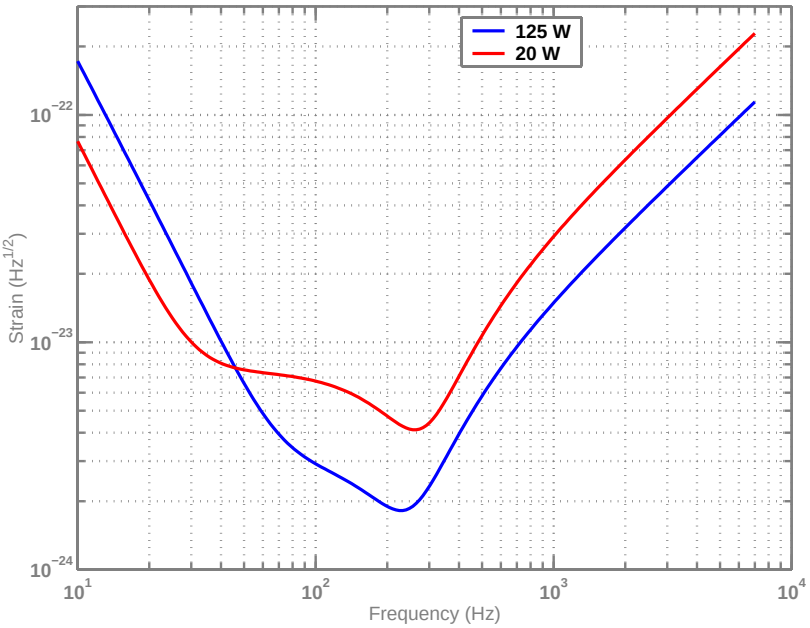

Figure 4. Strain sensitivity for the sapphire reference design at an interferometer input power (incident on the power recycling mirror) of 125 W (nominal design) and 20 W (giving improved sensitivity below 45 Hz).

The input power will be controlled just before the beam's entry into the vacuum system. Thus the mode cleaner and all downstream interferometer components must be designed for operation at 125 W and 20 W. All subsystem performance requirements must be met at both power levels, implying that technical noise in the 10-40 Hz band must be controlled relative to the lower strain spectrum, and any thermal distortion compensation may need to be adaptable to these limits.

4.5. Test mass material

In the critical frequency region around 100 Hz, thermal noise of the test masses either dominates or is a significant fraction of the noise budget. This noise source is predominantly governed by materials properties; two test mass materials are being considered: fused silica and sapphire. A sapphire-based design gives modestly improved performance in terms of the NBI figure of merit (~20% larger range), and could have significantly better thermal performance, depending on how low sapphire's absorption coefficient can be made. However there are still significant technical barriers and unknowns in developing sapphire that meets our requirements. Thus the baseline design calls for sapphire test masses, but with fused silica pursued as a viable fallback. The final selection is planned to occur in mid-2002, chosen to be early enough to accommodate the long core optic production cycle.

4.6. Test mass size and mass

To reduce the effect of radiation pressure (both of quantum and technical origin), the mass should be made as large as possible. In addition, the noise incentive of a large spot size in the case of sap-

phire supports the push to larger test mass size. The interferometer performance (NBI range) for different test mass masses is shown in Figure 5, for both sapphire and fused silica.

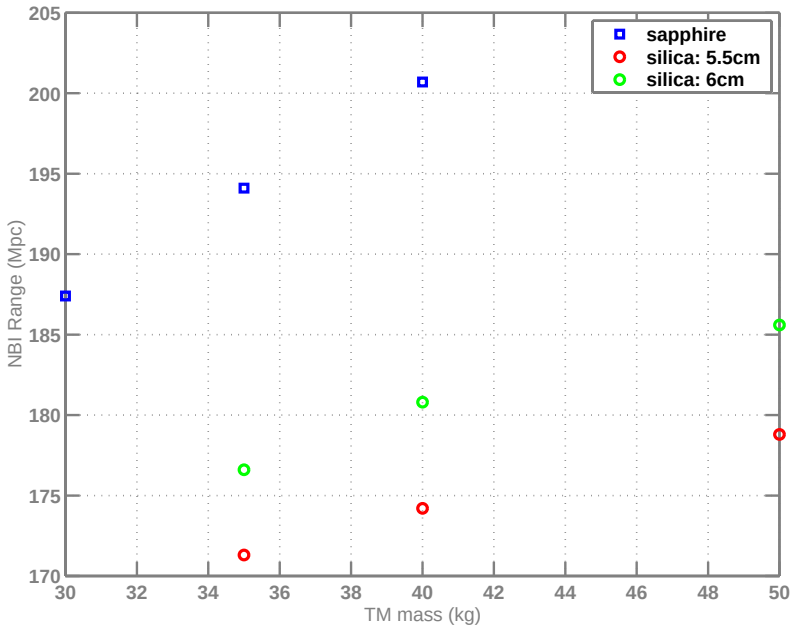

Figure 5. NBI range versus mass of the test masses. For each mass, the aspect ratio of the mirror has been optimized; sapphire is assumed to have an availability limit of 40 kg). The beam size is chosen such that the effective aperture loss at each mirror size is 15 ppm per mirror, up to a maximum beam size of 6.0 cm for sapphire, and either 5.5 cm or 6.0 cm for fused silica, as shown. The mirror Q is taken to be 200 million for sapphire, 30 million for silica (i.e., omits current coating loss estimates). The signal recycling parameters are also optimized at each point.

For sapphire, 40 kg is the largest mass (in round numbers) that the grower Crystal Systems believes is possible to ‘mass produce’ in our time frame. Achieving this size is still a development project for Crystal Systems. Their current 13.5 inch diameter production boule can conservatively produce a ϕ28cm×10cm piece (25 kg), and optimistically a ϕ30cm×12cm piece (34 kg). Hopeful for success growing larger diameter boules, we specify 40 kg as the baseline mass for sapphire.

For fused silica, the limit would be determined more by the size that could feasibly be polished, coated, and suspended. The bulk material is available in very large sizes: Heraeus’ brochure gives 80 kg as the largest mass for suprasil 312, but even this is probably not a firm limit; in the past they have supplied pieces (311 grade) larger than their listed maximum. The processing limitations have not yet been fully explored; if fused silica is selected as the test mass material, the specific choice of mass will be made based on these issues and performance estimates.

4.7. Beam size

For both sapphire and fused silica the internal thermal noise decreases with increasing beam size on the mirror–as $1/\omega^{3/2}$ for thermo-elastic noise (dominant for sapphire) and $1/\omega^{1/2}$ for internal friction (and coating) loss (dominant for fused silica). There are several limiting factors to increasing the beam size:

- aperture loss in the arm cavities, given the size available/chosen for the test masses

- ability of the polishers to produce very long radius of curvature within the tolerances
- ability of the polishers to produce the required uniformity over a larger central area
- stability of the arm cavities with a small $(1 - g)$ parameter and the recycling cavities, in the presence of mirror distortions (polishing and thermal) and misalignments

For sapphire, the limiting constraint appears to be aperture loss, given our assumed limit for the material size (for a given mass, thermoelastic noise becomes worse when the mirror gets too thin, even if the beam size is increased proportionally to fill the mirror). Applying an upper limit to the effective aperture loss of 15 ppm per mirror, thermal noise in a 40 kg piece of sapphire is minimized for a beam radius of 6.0 cm (see section 6.4.); this is our baseline beam size. A 6.5 cm radius beam on this same optic (30 cm optical aperture) would experience nearly 60 ppm of aperture loss per mirror.

For fused silica the choice is less clear, in part because the dependence on beam size is weaker. Aperture loss is not the issue, since the mirror diameter can be relatively large. The mirror production and cavity stability issues are the relevant constraints; these need further study before determining a best choice of beam size.

4.8. Low frequency cutoff

The seismic cutoff frequency (or ‘seismic wall’) is the frequency at which seismic noise, steeply falling with frequency as filtered by the seismic isolation and suspension subsystems, moves the test masses by the same amount as the predominant fundamental noise source(s), be it quantum radiation pressure or suspension thermal noise.

The seismic cutoff frequency is specified to be 10 Hz. This choice is based partly on its impact on predicted source sensitivities, and partly on technical feasibility. The effect of cutoff frequency on the NBI range and the stochastic background is shown in Figure 6. Neither source is significantly affected for cutoff frequencies in the range 10-15 Hz. Detection of BH-BH mergers of intermediate mass is probably more sensitive; the maximum binary mass that can be detected scales inversely with the seismic wall frequency. K Thorne has estimated the impact of the cutoff frequency on this source, see LIGO-T000146-00. The lack of event rate information makes it difficult to firmly quantify; Thorne argues that it would be unwise to make the cutoff frequency as

high 20 Hz, but that a 12-13 Hz wall would be unlikely to have a significant impact on intermediate mass BH-BH detection.

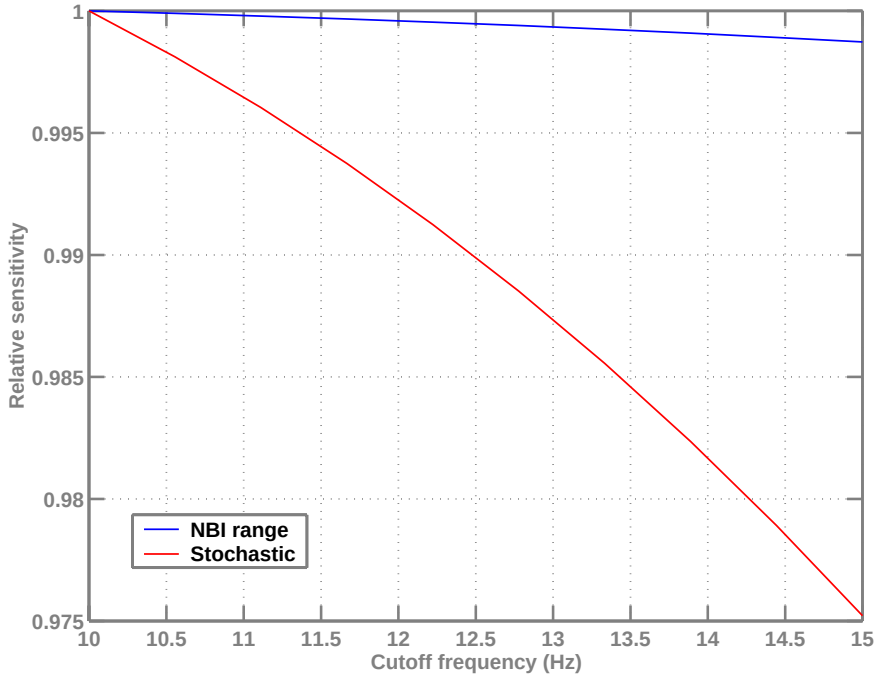

Figure 6. The sensitivity for NBI and stochastic background detection, relative to the sensitivity level at 10 Hz.

Given the conceptual designs of the seismic isolation and suspension subsystems, the technical limit to lowering the seismic wall comes from the vertical resonance of the last stage of the suspension: the stiffness is essentially that of the fused silica suspension fiber, whose minimum cross section is dictated by the suspended mass and the fiber strength; the effective mass is approximately that of the test mass (m_{tm}), reduced by that of the penultimate mass (m_{tm}): $m_{\mathrm{eff}} = m_{\mathrm{tm}} m_{pm} / (m_{\mathrm{tm}} + m_{pm})$. To get an idea of the numbers, take the following approximation for the vertical mode frequency:

$$\omega^2_{\mathrm{v}} \approx \left(\frac{gY}{L}\right)\left(\frac{m_{\mathrm{tm}} + m_{pm}}{m_{pm}}\right)\left(\frac{1}{fS_{\mathrm{b}}}\right)$$

where Y is the Young's modulus, S_{b} the breaking stress, and L the length of the fiber, g is the gravitational acceleration, and f is the fraction of the breaking stress at which the fiber is loaded. For fibers 0.6 m long and loaded at 25% of their breaking stress ($S_{\mathrm{b}} \approx 2$ GPa), the vertical frequency ranges from 7.6 Hz for an infinite m_{pm}, to 10.7 Hz for m_{pm}=m_{tm}, to 13.2 Hz for m_{pm}=m_{tm}/2 (as would roughly be the case for a sapphire test mass and a silica penultimate mass of the same size).

It remains a challenge for the suspension design to achieve a sub-10 Hz vertical frequency; by using a dense glass for the penultimate mass it appears to be feasible, without resorting to a composite (glass-metal) penultimate mass (risky for non-gaussian noise production). The allowed

level of ground noise at 10 Hz, and the division of seismic isolation between the seismic isolation and suspension subsystems is given in section 5.3.

4.9. GW Channel Readout

There are two candidate schemes for detecting the gravitational-wave signal sidebands at the output port: an rf readout, similar to initial LIGO, where phase modulation sidebands applied to the input laser beam are arranged to transmit to the output port, and are used to heterodyne detect the signal; a dc readout, where the Michelson is operated with a slight offset from the dark fringe, and the signal shows up as a baseband intensity modulation of the carrier (homodyne detection).

The dc readout scheme appears to be favored in all technical implementation considerations. The essential comparison still pending is that of their quantum-limited sensitivity. It is possible that the rf readout will have a significantly better quantum-limited sensitivity; this would likely trump the dc readout's practical superiority. Until the analysis is completed and the choice made, technical noise sources that depend on the readout scheme are specified for the worst case (rf readout) scenario.

5 SYSTEM LEVEL NOISE SOURCES

5.1. Fundamental noise sources

The interferometer performance is designed to be limited by fundamental noise sources–quantum noise and thermal noise. While these arise from fundamental physical mechanisms and cannot be 'engineered away', they depend on parameters that must be carefully controlled in order to achieve the target noise levels. This section gives requirements on parameters affecting the fundamental noise sources.

5.1.1. Quantum noise

Photodetector quantum efficiency. In principle a less-than-unity quantum efficiency can be compensated by an increase in input laser power. While more laser power may be available, the interferometer will likely already be operating near its thermal limit; unlike losses in the interferometer, for which a compensating increase in the input power just makes up for the lost stored power, photodetector losses (including any loss in the antisymmetric port path) would have to be compensated by an increase in stored arm power. Thus one cannot arbitrarily trade-off photodetector efficiency for input power.

The requirement for detection efficiency at the gravitational wave signal port is established at 90%. This includes photodetector efficiency, and the transmission of any optics between the signal recycling mirror and the photodetector. Assuming no compensating increase in input laser power, this reduces the NBI range by about 2%.

Readout scheme.

5.1.2. Internal thermal noise

Ideally, internal thermal noise is dictated by intrinsic properties of the test mass substrate material. However, the internal mechanical loss of the substrate material may be degraded by polishing or the addition of coatings or attachments; currently the most severe effect comes from the optical coating. Present estimates are that the coating mechanical loss is approximately 4×10^{-4}, which would lower sapphire's effective Q from 200×10^6 to about 4×10^6. This reduces the NBI range significantly from 200 Mpc to 144 Mpc. Ideally we would require that any such operations on the test mass material have a minimal impact on the performance, reducing the NBI range by less than 5%, e.g. (for sapphire, this would require an effective $Q > 40\times10^6$). Given the infant state of our knowledge of the mechanical properties of coatings (and the fact that there is no alternative to multi-layer dielectric coatings!), it is unclear if this goal can be met.

On the other hand, the thermal expansion and conductivity coefficients measured in sapphire–which determine the level of thermo-elastic surface fluctuations–appear to be properties of the crystal, not amenable to engineering. The factor that is under our control is the beam size (and shape, in principle) on the test masses. In the advanced LIGO design we use a TEM_{00} mode, and strive to make it as large as feasible. We are not pursuing the proposed 'flat-top' beam profile which can further reduce thermo-elastic noise; it is deemed to be too undeveloped and risky for this design.

5.1.3. Suspension thermal noise

Suspension thermal noise is also largely dictated by properties of the suspension fiber material. One parameter under control is the stress level in the fiber; this should be chosen to avoid significant non-gaussian energy release (creep). Another controllable parameter is the shape of the fiber; for the same fiber cross section, making the fiber thinner in the direction of the optic axis makes it more compliant and thus less lossy for motions along that direction.

Calculations of the loss for a round fiber and a ribbon-shaped fiber having a 1:10 aspect ratio (at the limit of feasibility) indicate that the thermal displacement noise for the ribbon would be approximately a factor of 2 lower than for the round fiber. To date however ribbons have proven to be difficult to make and not as strong as round fibers, thus their noise benefit must be analyzed carefully for its impact on performance, and weighed against their practical risks. In the high-power mode, the lower noise afforded by ribbons is insignificant, since thermal noise with round fibers is already significantly lower than quantum and internal thermal noise. In the low-power mode, ribbons would afford a small improvement (~10%) in the stochastic background sensitivity.

We conclude that the relatively small performance advantage possible with ribbons does not outweigh their present risks, and do not require the test mass suspensions to use them. This does not rule out using ribbons if their current technical difficulties are overcome.

5.2. Technical noise

All technical noise sources must be controlled so that the equivalent strain noise (amplitude spectral density) of each such source is no more than 10% of the target strain sensitivity. This applies across the entire gw band of 10 Hz-7 kHz, and to both the low and high power modes of operation. At this level a single noise source would degrade the strain sensitivity by 0.5% (though not

all technical noise sources will be significant over the whole gw band); there may be ~10 technical noise sources that are significant in a given frequency region, degrading the strain sensitivity by 5%. For noise sources that are independent of the input power, we form an equivalent-strain technical noise spectrum that is 10% of the minimum of the low power-high power strain curves at each frequency. This technical noise strain limit is shown in Figure 7. Noise sources that depend on the input power (such as technical radiation pressure) must each be no more than 10% of the relevant curve of Figure 4, for both power levels.

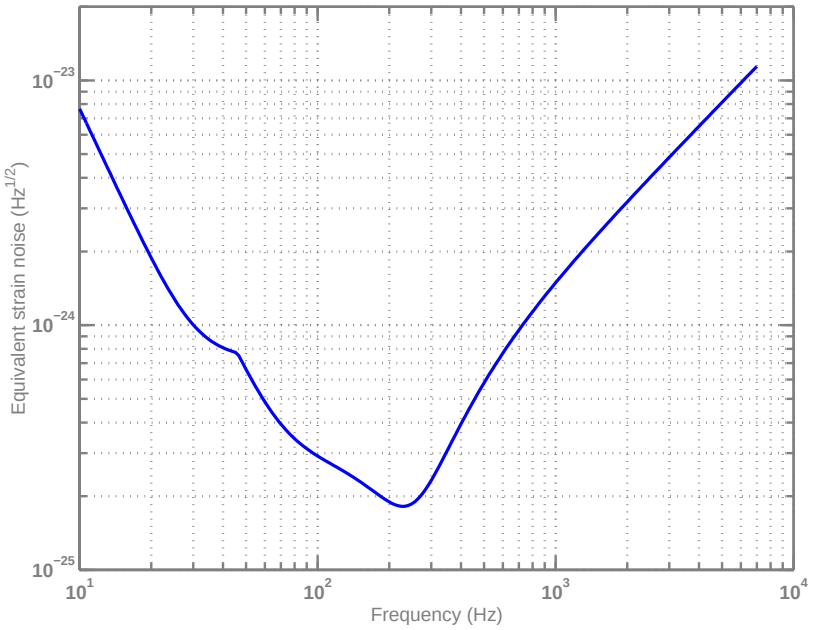

Figure 7. Equivalent strain noise limit for technical noise sources. The curve is 10% of the minimum of the two curves shown in Figure 4, and applies to technical noise sources that are independent of the input power.

5.3. Ground noise

Ground noise isolation is provided by the seismic isolation and suspension subsystems. This section gives the isolation requirement at 10 Hz, since this involves a trade-off between these two subsystems. A 10 Hz specification suffices for the entire gw band, since ground noise falls so quickly at these frequencies; ground noise isolation at lower frequencies is dealt with later. There are different isolation requirements for the various suspended optics, depending on how strongly they couple to the gw channel. Since optics with different requirements may be mounted on the same seismic isolation platform, and the various seismic isolation platforms can be designed to perform at the same level, the isolation variability is all passed on to the suspensions.

The seismic isolation platforms must all meet a displacement noise requirement of 2×10^{-13} m/$\sqrt{\text{Hz}}$ at 10 Hz, in all three translational degrees-of-freedom.

The 10 Hz displacement noise levels given below apply with the suspension's local damping active for all degrees-of-freedom of all optics except the test masses, where interferometer signals can be used to control the longitudinal degrees-of-freedom (damping of other degrees-of-freedom should remain active). This is over constraining, since there will be 5 interferometer signals that

could be used to damp 5 of the interferometer (core) optics (and one to damp one of the mode cleaner mirrors). However for flexibility we specify the requirements so that any of the non-test mass optics can remain locally damped. If this proves difficult to meet, we may be able to choose other optics to leave locally undamped during operation.

5.3.1. Test masses

For each of the four test masses, the displacement noise must be held to 1×10^{-19} m/$\sqrt{\text{Hz}}$ or lower at 10 Hz. This applies to the combined effect of motion along the optic axis and vertical motion multiplied by a cross-coupling factor of 0.1%. As previously stated, local damping of the suspension's longitudinal degrees-of-freedom are not required to be active when this requirement must be met.

The resulting strain noise from four test masses is $5\times10^{-23}/\sqrt{\text{Hz}}$, roughly 30% and 60% of the target strain sensitivity at 10 Hz for the high-power and low-power cases, respectively.

5.3.2. Beamsplitter

Beamsplitter motion should be made negligible compared to test mass motion. The effect of beamsplitter motion on the output is smaller than that of the test masses by a factor $\sqrt{8}F/\pi \approx 1100$, so the displacement noise requirement at 10 Hz is 2×10^{-17} m/$\sqrt{\text{Hz}}$. This applies to the combined effect of motion along the optic axis and vertical motion multiplied by a cross-coupling factor of 1.4% (surface normal angle determined by optical layout design).

5.3.3. Recycling mirrors

The displacement noise requirement for the power recycling mirror (PRM) is derived based on its effect on the frequency sensing, as follows:

- worst case (rf readout) input beam frequency stability requirement is 5×10^{-7} Hz/$\sqrt{\text{Hz}}$ at 10 Hz (including factor of 10 margin for technical noise)
- this corresponds to arm cavity displacement noise of 7×10^{-18} m/$\sqrt{\text{Hz}}$
- the reflection port sensing is 43 dB less sensitive to PRM motion than to arm common motion at 10 Hz
- add another factor of 3 margin, so that PRM motion is a small part of the frequency stability budget

The resulting PRM displacement noise requirement is 3×10^{-16} m/$\sqrt{\text{Hz}}$ at 10 Hz. This applies to the combined effect of motion along the optic axis and vertical motion multiplied by a cross-coupling factor of 0.6% (surface normal angle determined by optical layout design).

A similar calculation is done to determine the sensitivity to signal recycling mirror (SRM) motion:

- introduce loss differences and small length offsets into the arms to model a dc readout scheme
- compare the detection port signal produced by differential arm motion to that produced by SRM motion
- require that SRM motion show up at the detection port at 1/10 the level of differential arm motion

The resulting displacement noise limit for the SRM is using this criterion is actually more lax than the above PRM requirement. Since the suspension designs for the PRM and SRM are the same, there is probably no benefit to retaining a more lax requirement for the SRM, and the stricter displacement noise requirement of 3×10^{-16} m/$\sqrt{\text{Hz}}$ at 10 Hz is applied to both mirrors. The vertical-horizontal cross-coupling coefficient for the SRM is 0.6%.

5.3.4. Input telescope mirrors

Motions of the reflective optics between the input mode cleaner and the PRM (telescope and steering mirrors) can be relatively large. Doppler-shift frequency fluctuations should be smaller than the required MC frequency stability (see section 5.4.); this sets a displacement noise limit of $\delta x(f) < 0.1(\delta\nu_l/\nu_l)(c/2\pi f) = 5\times10^{-11}$ m/$\sqrt{\text{Hz}}$ at 10 Hz–a level actually above the seismic platform motion. The angular pointing stability of the beam incident on the PRM must be ~1 prad/$\sqrt{\text{Hz}}$ or better (see section 5.6.). Even assuming a large displacement-to-angle cross-coupling of 1 rad/m, the implied displacement noise is only <1 pm/$\sqrt{\text{Hz}}$.

5.3.5. Output telescope mirrors

TBD

5.3.6. Compensation plate

TBD

5.4. Laser frequency noise

Laser frequency noise couples to the gw channel through differences in the arm losses and input mirror transmissivities; it thus involves a trade-off between core optics requirements and frequency stability, the latter involving further trade-offs among three subsystems. The allowed frequency noise at the PRM is calculated[1] using a round trip loss difference between the arms of 20 ppm, and a fractional difference in the input mirror transmissions of 1%. The result is shown in Figure 8, for both candidate readout schemes.

Also shown are frequency noise requirements for the pre-stabilized laser (PSL) and mode cleaner (MC). The advanced LIGO interferometers will use a three-level frequency stabilization hierarchy, similar to initial LIGO: the laser is first stabilized to a reference cavity; the PSL is then stabilized to the MC; the MC output is stabilized to the arm cavities. The requirements for the first two stages have been chosen using two guidelines: the frequency suppression required at high frequencies gets smaller for successive stages in the stabilization hierarchy–this eases the gain requirements for the loops which naturally have lower bandwidths; the suppression required at low frequencies for the last two stages is made relatively large–this anticipates the possibility that the cavity lengths (mode cleaner and arm common mode) are stable enough at low frequencies that the last two stabilization levels will not require feedback to the cavity lengths. In this case the

1. calculations performed with Jim Mason's matlab routines; see his Ph.D. thesis for details

full open loop gain of a given stage can be effective in suppressing frequency noise, and the frequency stability required from the previous stage can be relatively relaxed.

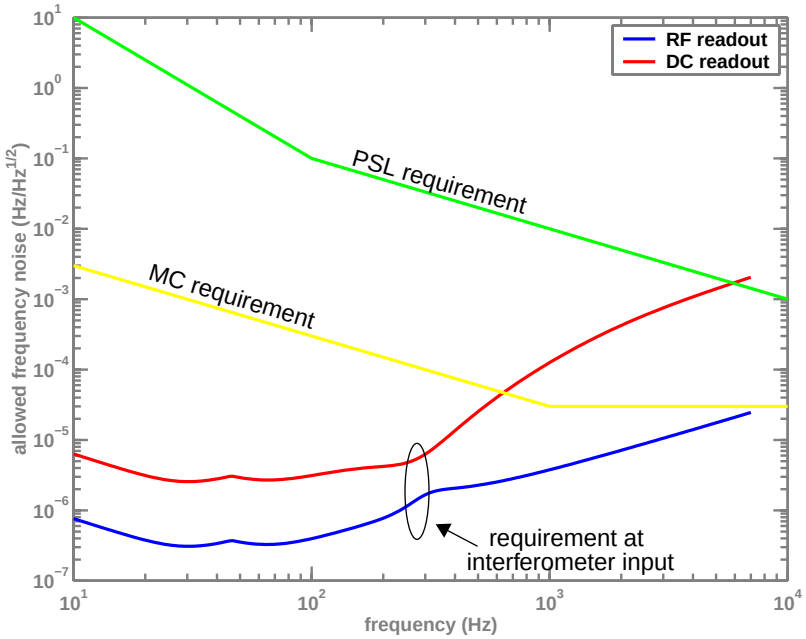

Figure 8. Allowed frequency noise at the interferometer input, calculated for rf (heterodyne) and dc readouts; the allowed level produces the equivalent strain noise shown in Figure 7. Also shown are the stabilization levels required from the pre-stabilized laser and mode cleaner stages.

5.5. Laser intensity noise & technical radiation pressure

Laser intensity noise couples to the gw channel through two mechanisms: the fluctuating radiation pressure in the arms does is not perfectly common mode if the average power in the arms is different; the sensing scheme will have some dependence on laser power, through an offset from the dark fringe or couplings through optical defects. The intensity noise requirement involves trade-offs between the PSL, COC and ISC subsystems.

The limit for the relative intensity noise on the beam incident on the PRM is shown in Figure 9. With a requirement on the balancing of the average arm cavity power of 1%, radiation pressure is the dominant mechanism below ~100 Hz. Since technical radiation pressure scales linearly with the input power (assuming a constant relative intensity noise), it is most significant in the high power operating mode. Above 100 Hz the coupling to AM depends on the sensing scheme. The rf readout is primarily dependent on the loss difference in the arms (20 ppm used), whereas the dc readout couples of course with the (intentional) differential length offset in the arms (5 pm used in this case).

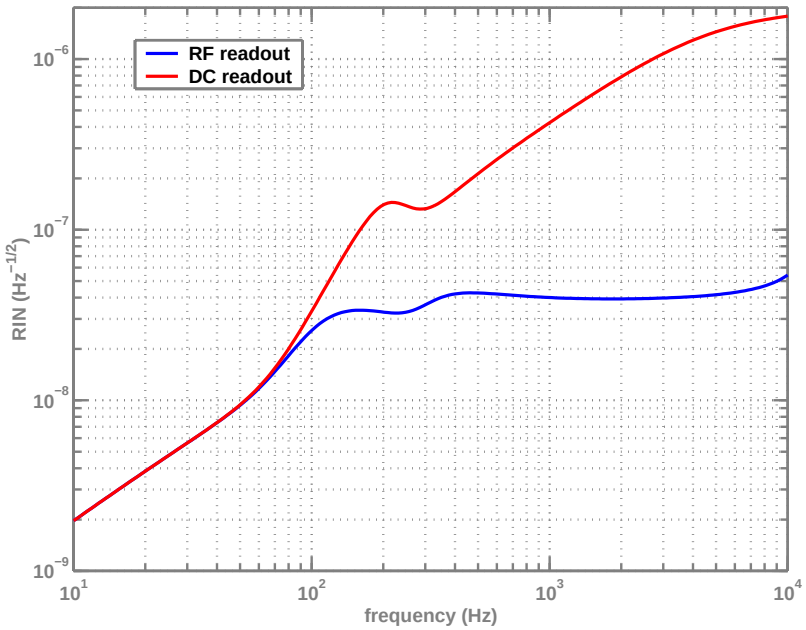

Figure 9. Relative intensity noise limit for the laser beam incident on the interferometer (PRM). With a 1% average power imbalance in the arm cavities, technical radiation drives the requirement at frequencies below ~100 Hz. The minimum photocurrent required to reach the 10 Hz stability requirement is $I_{\mathrm{dc}} = 2e/(\mathrm{RIN})^2 = 80\ \mathrm{ma}$.

5.6. Misalignment & Beam pointing noise

Fluctuations of the input beam direction couple to the gw channel with misalignments of the interferometer optics. The noise source involves trade-offs between three subsystems: IOO, responsible for stabilizing the beam direction; ISC, responsible for alignment control of the interferometer; SUS, responsible for suspension designs in the IOO chain.

Beam jitter coupling for the advanced LIGO configuration has been calculated by G Mueller; see G010154-00-Z. Pointing fluctuations of the input beam couple most strongly to a signal at the output via differential misalignments of the arm cavity mirrors. Mirror misalignments also degrade the sensitivity because they reduce the effective power in the interferometer. Once this has been analyzed, the results can be combined with the beam jitter calculation to determine the trade-off between alignment and beam jitter requirements. Given the amount of seismic isolation provided by SEI in the ~1-10 Hz band, it is likely to be feasible and worthwhile to significantly tighten the initial LIGO misalignment tolerance of 10^{-8} rad-rms.

6 Subsystem Requirements & Conceptual Design

6.1. Prestabilized laser

The following hardware and functions are within the scope of the PSL subsystem:

- Nd:YAG laser, 1064 nm wavelength, single frequency, with sufficient power to meet the

PSL output power requirements
- frequency pre-stabilization of the PSL output beam
- intensity stabilization of the mode cleaner output beam
- frequency actuation inputs, for subsequent frequency control
- amplitude and frequency modulation inputs, for global diagnostics

The primary requirements of the PSL are given below.

Output power	
TEM_{00} mode	165 W
Higher order mode power	< 5 W
Stability. long term, over any 24 hr period	+/– 1%
Intensity stability	
gw band	see Figure 9
control band, 0.1 Hz < f < 10 Hz	< 0.1% rms
Frequency stability	
gw band	see Figure 8
control band, 0.1 Hz < f < 10 Hz	< 5 kHz rms
Technical AM at the modulation frequency	TBD
Modulation inputs	
power	10 kHz BW, +/–1% range
frequency, wideband input	BW: <20° lag at 100 kHz, range: DC-1Hz: 1 MHz p-p; f >1 Hz: 10 kHz p-p
frequency, tidal input	range: 50 MHz p-p speed: time constant < 30 min

Table 2: Primary requirements for the pre-stabilized laser (PSL).

6.2. Seismic Isolation

Refer to E990303-03-D.

6.3. Input optics

The scope of the input optics subsystem includes:

- modulators required for the interferometer sensing scheme
- input mode cleaner
- mode matching telescope to match input beam to interferometer mode
- static power control of the input beam
- provide the interferometer reflected beam, the mode cleaner reflected beam, and a sample of the mode cleaner transmitted beam to detection ports
- provide the required input beam pointing stability

- provide isolation of the interferometer reflected beam from the laser

The primary requirements for the input optics are given below.

Output power	
at mode cleaner output, TEM_{00} mode	125 W
matching of TEM_{00} mode to arm cavity mode	> 98%
higher order mode content	< 1 W
Frequency stability	
gw band	see Figure 8
control band, 0.1 Hz < f < 10 Hz	TBD
Mode cleaner length	16 m
Beam pointing stability	TBD

Table 3: Primary requirements for the input optics (IOO).

6.4. Core optics

The scope of the core optic components (COC) subsystem includes:

- procurement of all interferometer optics (four test masses, beamsplitter, power and signal recycling mirrors, fold mirrors where applicable)
- metrology of all core optics (high reflectivity surfaces; substrates of input test masses and beamsplitter)
- specification of cleaning procedures for core optics

The primary requirements for sapphire test masses are given below.

Test masses	
material	sapphire
physical diameter/ optical aperture	31.4 cm/ 29.8 cm
thickness	13 cm
bulk absorption, input test masses	< 20 ppm/cm
HR surface radius of curvature, tolerance	55 km, tolerance TBD
input test mass transmission	0.5% (+/–0.05%; pairs matched to 1%)
HR surface absorption	< 0.5 ppm
effective arm cavity round trip loss	< 75 ppm
bulk homogeneity, central 200 mm diam, ITMs	< 20 nm (double pass)

Table 4: Primary COC requirements for the test masses.

The aspect ratio of the test mass has been chosen to minimize internal (thermo-elastic) thermal noise. Figure 10 shows the internal thermal noise at 100 Hz versus the thickness of the test mass, keeping constant: the mass, at 40 kg; the ratio of aperture radius to beam size, at 2.49, which produces an effective aperture loss of 15 ppm per mirror. Internal thermal noise is minimized at a thickness of 13 cm, for which the beam radius is 6.0 cm.

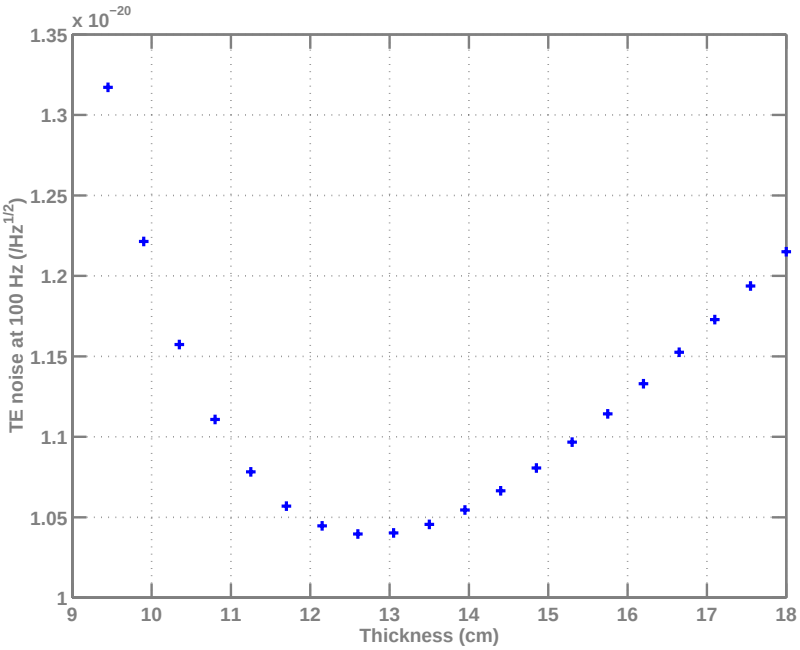

Figure 10. Internal thermal noise level at 100 Hz for a 40 kg test mass as a function of its thickness. At each point the ratio of the aperture radius (physical radius minus 8 mm) to the beam radius is fixed at 2.49, corresponding to 15 ppm of effective aperture loss per mirror. At t = 13 cm, the beam radius is 6.0 cm.

Another COC issue that affects interferometer performance is degradation of the internal mechanical loss of the substrate material by polishing or the addition of coatings or attachments; currently the most severe effect comes from the optical coating. Current estimates are that the coating loss is 4×10^{-4}, which would lower sapphire's effective Q from 200×10^6 to about 4×10^6. This reduces the NBI range significantly from 200 Mpc to 144 Mpc. Ideally we would require that any such operations on the test mass material have a minimal impact on the performance, reducing the NBI range by less than 5%, e.g. (for sapphire, this would require an effective $Q > 40\times10^6$). Given the infant state of our knowledge of the mechanical properties of coatings (and the fact that there is no alternative to multi-layer dielectric coatings!), it is unclear if this goal can be met.

Primary requirements for the other core optics are given below. Many of the optical specifications are simply current estimates; more modeling is needed to firm these up. The main effect of losses in these optics is to reduce the power recycling factor. The power loss from the arms (T = 0.5%, round trip loss = 75 ppm) is 6%, and the additional loss from the power-recycling cavity optics should be a small fraction of this: less than 0.3% is specified (this includes contrast defect loss and loss from the ITM AR surfaces, so it actually involves more than just the beamsplitter and power

Beamsplitter	
material	fused silica
physical diameter	35 cm
thickness	TBD
bulk absorption	< 0.5 ppm/cm
R/T tolerance	(R – T) < 0.5%
Recycling mirrors	
material	fused silica
physical diameter/ optical aperture	26.5 cm/ 24.5 cm
thickness	10 cm
bulk absorption (PRM)	< 15 ppm/cm
Round trip loss in the PRM, carrier (not including 6% loss from arms)	< 0.3%

Table 5: Primary COC requirements for the beamsplitter and recycling mirrors.

recycling mirror). The optical requirements will be refined based on this round trip loss requirement.

6.5. Suspensions

The scope of the suspensions subsystem includes:

- suspension mechanics for all core optics, up to the attachment points on the optic
- procurement and bonding of attachments to core optics for suspension points
- local damping of all suspension rigid body modes
- local sensing of the suspension
- actuation capability for global control
- suspension designs for input and output optical components (mode cleaner and telescope mirrors, e.g.)

The primary requirements for the test mass suspensions are given below. Similar requirements for all other suspended components are being determined.

Test masses	
optic axis motion from ground noise + local damping noise, at 10 Hz	$<10^{-19}$ m/√Hz
optic axis motion from thermal noise at 20 Hz	$<2\times10^{-20}$ m/√Hz
suspension rigid body eigenfrequencies	must be lower than 10 Hz
maximum Q's of rigid body modes	TBD
global actuator characteristics	TBD

Table 6: Primary SUS requirements for the test mass suspensions.

6.6. Interferometer Sensing & Control

The scope of the interferometer sensing and control subsystem includes:

- the controls systems for the input and output mode cleaners
- sensing of all interferometer length degrees-of-freedom, including readout of the gravitational-wave signal
- lock acquisition of the interferometer
- lock maintainence at the interferometer operating point
- output mode cleaner design
- sensing and control of the interferometer alignment

6.7. Auxiliary Optics Support

The scope of the auxiliary optics support subsystem includes:

- beam dumps and light baffling for the interferometer
- beam reducing telescopes for auxiliary beams
- initial alignment surveying and support
- optical levers for all core optics
- active thermal compensation for the core optics
- photon actuators for the end test masses

APPENDIX A SENSITIVITY WITH FUSED SILICA TMS

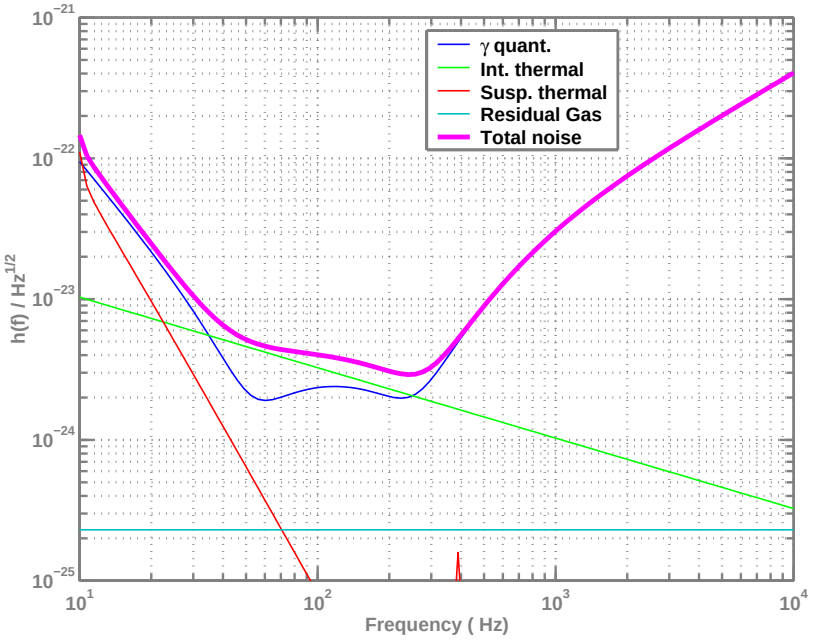

Figure 11. Estimated strain sensitivity using 40 kg fused silica test masses (calculated with BENCH, v. 1.10). Input laser power is 80 W, 530 kW in the arm cavities. Beam size is 5.5 cm radius. The neutron-star binary inspiral detection range for a single such interferometer is 176 Mpc.